LASER & PHOTONICS REVIEWS
www.lpr-journal.org

Metal-Insulator-Semiconductor Structure-Based InGaN/GaN Micro-Light-Emitting Devices with Superior External Quantum Efficiency

*Jian Yin, Reza Chaji, Ding Li, Zhong Lin Wang, Md Soyaeb Hasan, and Dayan Ban**

In this article, InGaN/GaN micro-light-emitting diodes (micro-LEDs) with innovative device structures are fabricated to suppress surface nonradiative recombination and improve device efficiency. A metal-insulator-semiconductor (MIS) sidewall structure enables the application of sidewall bias to adjust the surface recombination of micro-LEDs. MIS micro-LEDs with various mesa dimensions are fabricated and characterized. Current density-voltage (*J-V*) measurements show the increase in surface defects-assisted tunneling current is attributed to a positive sidewall bias lowering the energy difference between the surface defect states and electron energy states, thereby decreasing the surface recombination and enhancing the external quantum efficiency (EQE) of the device. The increase or decrease in measured device EQE is approximately proportional to the magnitude of the positive or negative sidewall bias, which is well-explained by the analytical model. The EQE of the MIS micro-LED with a mesa dimension of 8 μm can be enhanced from 20.0% to 30.7% at a low injection current density (0.625 A cm^{-2}) by applying a +20 V sidewall bias, which is comparable to the performance of state-of-the-art organic-LEDs (OLEDs). More importantly, the maximum EQE of the 8 μm MIS micro-LED is measured to be ≈53.9% at 23.3 A cm^{-2}, which is the highest reported EQE to the best of the knowledge.

1. Introduction

Ever since the indium gallium nitride/gallium nitride (InGaN/GaN) blue LED was first demonstrated in the 1990s, it has become one of the most popular light sources for various applications. The InGaN/GaN blue LED offers several advantages, including high efficiency, high brightness, low power consumption, good chromaticity, and long lifetime, all of which meet the requirements for high-resolution displays. The primary drawback of InGaN/GaN LEDs is the so-called efficiency droop, which refers to the reduction of efficiency as the current increases. The primary origin of efficiency droop is the carrier recombination out of the active region due to the disparity in mobilities and concentrations between electrons and holes.[1–3] This issue has been significantly mitigated by developing an electron blocking layer (EBL) between the active region and the p-GaN region.[4,5] Therefore, InGaN/GaN blue micro-LEDs were considered the most promising candidates for high-resolution display pixels a few years ago.

However, as the miniature high-resolution displays developed, OLED displays gradually dominated the electronic market. The latest electronic products from Apple, Samsung, or other consumer electronics companies, including smartphones, smartwatches, tablets, laptops, virtual reality (VR) and augmented reality (AR) applications, either already use or plan to use OLED displays. One of the main factors contributing to the low competitiveness of InGaN/GaN micro-LED displays is the observed EQE degradation as the size of micro-LEDs decreases. **Figure 1a** shows the peak EQE versus current density for several reported state-of-the-art OLEDs from[6–13] and state-of-the-art InGaN/GaN micro-LEDs from.[14–19] While the maximum EQE values of micro-LEDs are comparable to those of OLEDs, the current density values required to achieve peak EQE are significantly higher for micro-LEDs than for OLEDs. At a current density of 1 A cm^{-2}, the EQE values of blue InGaN/GaN micro-LEDs reported in[16–19] drop below 1%. However, micro-LEDs can still achieve a luminance of thousands or even tens of thousands cd m^{-2} at 1 A cm^{-2}, exceeding the highest luminance requirements for high-resolution display applications. Figure 1b presents the EQE values of OLEDs

J. Yin, M. S. Hasan, D. Ban
Department of Electrical and Computer Engineering
Waterloo Institute Nanotechnology
University of Waterloo
Waterloo, ON N2L 3G1, Canada
E-mail: dban@uwaterloo.ca
R. Chaji
Vuereal InC.
440 Philip Street, Unit 100, Waterloo, ON N2L 5R9, Canada
D. Li, Z. L. Wang
Beijing Institute of Nanoenergy and Nanosystems (BINN)
Chinese Academy of Sciences (CAS)
Beijing 101400, China

The ORCID identification number(s) for the author(s) of this article can be found under https://doi.org/10.1002/lpor.202500791

DOI: 10.1002/lpor.202500791

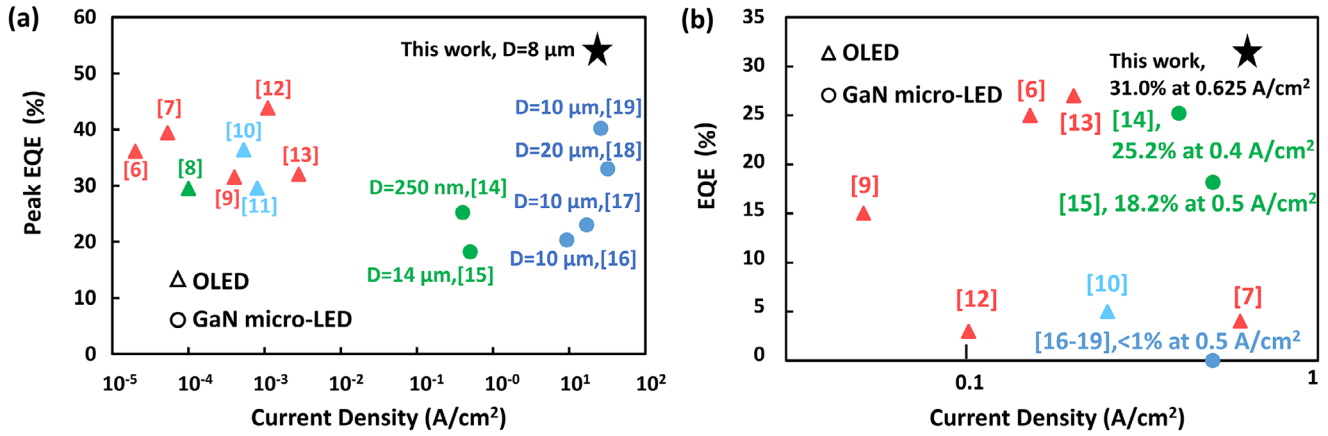

Figure 1. a) The extracted peak EQE versus current density of OLEDs with various colors (triangle markers) from published literature[6–13] and InGaN/GaN micro-LEDs with different mesa (circle markers) dimensions from.[14–19] The black marker is the peak EQE of MIS micro-LEDs with an 8 μm mesa dimension in this work. b) The extracted EQE values at <1 A cm^{-2} from.[14–19] The EQE values of OLEDs from[6–13] were at their highest measured luminance (≥ 10^4 cd/m^2). The black marker is the EQE value at 0.625 A cm^{-2} of MIS micro-LEDs with an 8 μm mesa dimension in this work. The red, green, blue colors represent the color of the emitted light from micro-LEDs.

from[6–13] at their highest measured luminance, all of which exceed 10^4 cd m^{-2}. In contrast, the EQE values of blue micro-LEDs in[16–19] at < 1 A cm^{-2} are significantly lower. The exceptions are the green quantum-dot (QD) micro-LEDs proposed in,[14,15] but they required expensive deposition techniques to grow the QDs, such as molecular beam epitaxy (MBE) and metal-organic vapor phase epitaxy (MOVPE). Consequently, the EQE degradation of InGaN/GaN micro-LEDs at low working current densities has replaced efficiency droop as the primary challenge limiting the market competitiveness of blue InGaN/GaN micro-LED displays. Despite this limitation, the unique advantages of InGaN/GaN systems, such as high brightness, fast response, slim thickness, and long lifespan, continue to propel research efforts toward achieving high-efficiency blue micro-LEDs.

In this work, we proposed micro-LEDs with metal-insulator-semiconductor (MIS) structures on the mesa sidewalls to improve the EQE performance. MIS micro-LEDs with various mesa dimensions (8, 15, 20, and 50 μm in diameter) were fabricated and characterized. The measured *J–V* curves indicated that applying sidewall biases lowers the energy gap between the surface defect states and the active region electron energy states, thus reducing the surface recombination velocity and increasing the EQE of the devices. Quantitative calculations based on our analytical model and measured EQE performance demonstrated that the increase or decrease in EQE is proportional to the sidewall bias applied to the MIS micro-LEDs. Specifically, the EQE at 0.625 A cm^{-2} for the 8 μm MIS micro-LED increased to ≈30.7% and the peak EQE was enhanced to ≈53.9% at 23.3 A cm^{-2}. The efficiency performance of this 8 μm MIS micro-LED is comparable to state-of-the-art OLEDs and surpasses any reported state-of-the-art InGaN/GaN micro-LEDs, as shown in Figure 1a,b.

2. Device Growth and Fabrication

The c-plane InGaN/GaN LED epitaxial structures were grown by metal–organic chemical vapor deposition (MOCVD) on a non-patterned 4″ sapphire substrate. The epi-layers and device geometry of the MIS micro-LEDs are shown in **Figure** 2b. The epi-layers consist of a GaN template layer, a 2 μm silicon-doped (Si-doped) n-GaN layer, an 18-period Si-doped superlattice, nine periods of InGaN/GaN multiple quantum wells (MQWs) and Si-doped quantum barriers (QBs), a 30 nm aluminum gallium nitride (AlGaN) EBL, a 70 nm magnesium-doped (Mg-doped) p-GaN layer, and a 220 nm indium tin oxide (ITO) layer. The ITO layer provides a good and transparent ohmic p-contact, which improves the device performance of the MIS micro-LEDs. The peak emission wavelength is ≈430 nm.

Before the fabrication process, a solvent sonification procedure was carried out to clean potential contamination. Following the cleaning steps, a silicon dioxide (SiO_2) layer and a chromium (Cr) layer, serving as the dry etching hard mask, were deposited on the wafer by plasma-enhanced chemical vapor deposition (PECVD) and electron-beam (e-beam) evaporation, respectively. The double-layer hard mask enhanced the quality of the dry-etched mesas by reactive ion etching (RIE). Circular mesas with dimensions of 50, 20, 15, and 8 μm (denoted herein as devices M50, M20, M15, and M8, respectively) were defined using ultraviolet (UV) lithography and etched through the ITO layer down to the n-GaN layer by RIE. During the RIE process, EKC265 post-etch residue remover was used to remove etching contamination thoroughly. The GaN RIE recipe required maintaining the boron trichloride (BCl3) ratio to chlorine (Cl_2) above 15% to ensure smooth mesa sidewall surfaces.[20] After dry etching, the mesas underwent sidewall treatment with piranha solution for 1.5 min at room-temperature, followed by potassium hydroxide (KOH) treatment for 30 min at 80 °C. The piranha solution formed a simple current aperture,[21] while the high-temperature KOH solution reduced sidewall surface defects and smoothed the mesa sidewalls of devices.[17–19,22]

After sidewall treatment, a 100 nm aluminum oxide (Al_2O_3) layer was deposited on the mesa sidewalls as the sidewall insulator layer in the MIS structure using atomic layer deposition (ALD). Al_2O_3 ALD is one of the most advanced sidewall passivation techniques and can effectively suppress surface defects on device sidewalls.[18] Following Al_2O_3 deposition, a ≈150 nm Al layer was sputter-deposited on the Al_2O_3 layer as the sidewall

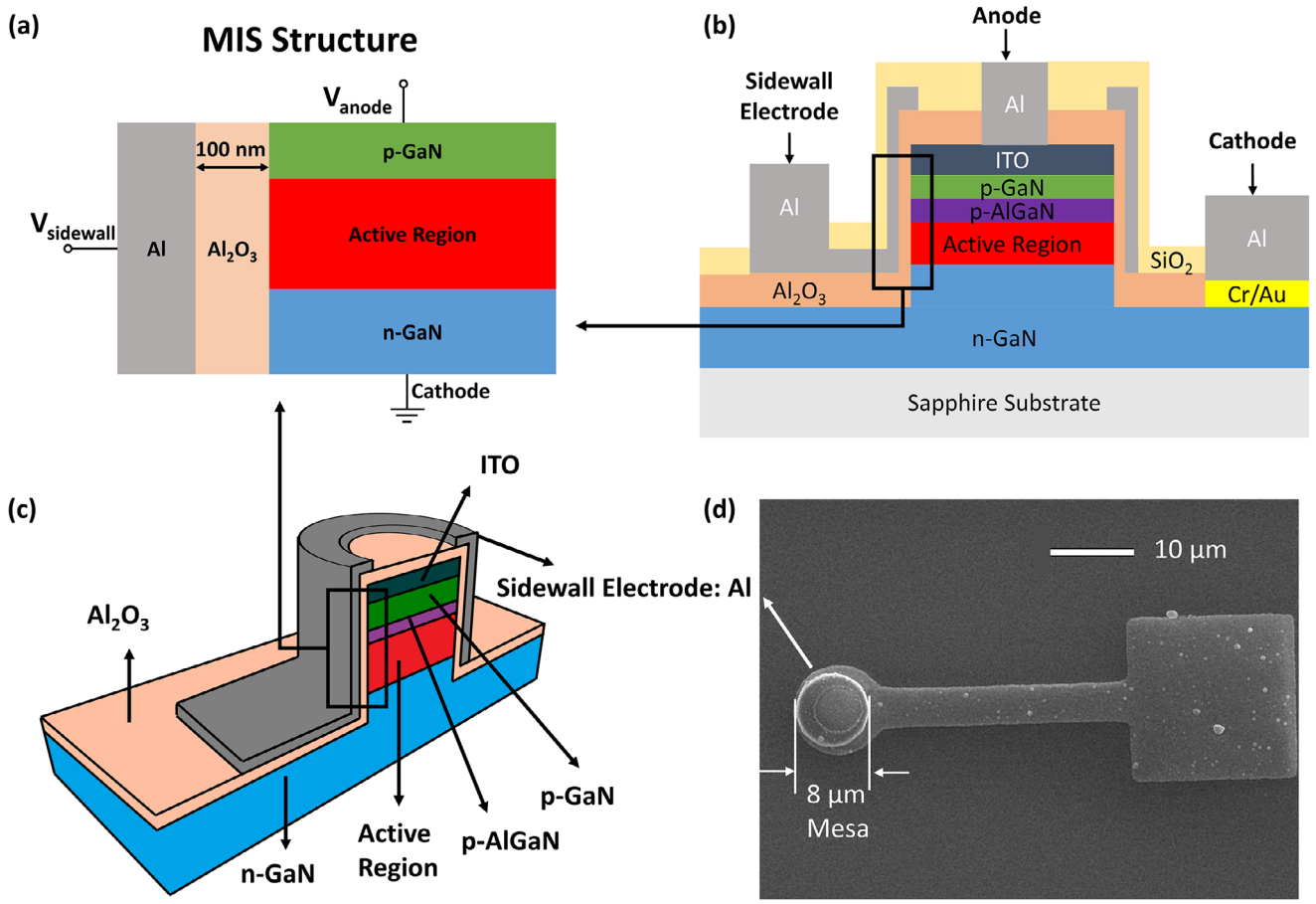

Figure 2. a) The schematic diagram of MIS structures on the mesa sidewall of the fabricated MIS micro-LEDs. b) Cross-sectional schematic of the epitaxial layers of fabricated MIS micro-LEDs. c) The 3D schematic diagram of the MIS structures; d) The SEM image of the ring-shaped sidewall electrode covered the 8 µm mesa.

metal layer in the MIS structure. The sidewall electrodes were then defined and etched by RIE. Figure 2a,c show the 2D and 3D cross-section schematic diagrams of the MIS structure on the sidewall of micro-LEDs. Figure 2d displays a top-view scanning electron microscope (SEM) picture of the sidewall electrode, showing an Al ring covering the mesa and its extended part for subsequent operations. The patterned Al sidewall electrodes were then protected by a 300 nm SiO_2 layer.

In the following fabrication process, selective areas of Al_2O_3 were removed by RIE to create electrode windows. The ohmic n-contacts were formed by depositing 30/10 nm of Cr/Gold (Au) via e-beam evaporation and a lift-off process. Moreover, a ≈750 nm Al layer was sputter-deposited on the wafer to ease subsequent wire bonding. The patterns of wire-bonding pads for three different electrodes were defined on the Al layer and etched using Al etchant D. Finally, the wafer was diced into 8 × 8 mm chips, which were mounted onto the designed printed circuit boards (PCBs) and wire-bonded for device measurement. Since the MIS micro-LEDs have three electrodes, a multi-channel source meter unit (SMU) was used to power the MIS micro-LEDs. Channel A of the SMU served as a current source connected to the anode of an MIS micro-LED, while channel B provided the voltage bias to the sidewall electrode. The cathode of the MIS micro-LED was connected to the common ground. The measurement setup used for the characterization of the MIS micro-LEDs is shown in **Figure 3**. The devices were operated in pulsed mode, and the emitted signal was collected using a Newport 818-UV/DB photodetector. The optical power measured using this setup was calibrated by comparing the EQE values obtained with a Labsphere 3P/4P-GPS-X general-purpose integrating sphere at our partner company. By carefully reproducing the measurement process and minimizing noise under completely dark conditions, the EQE values could be reliably measured in our laboratory.

3. Device Characterization and Discussion

Figure 4a shows the *J*–*V* characteristic curves of MIS micro-LEDs with various mesa dimensions, measured using a semiconductor parameter analyzer (4200A-SCS) with a shielding box and vibration isolation system. The analyzer has a noise floor of ≈10 fA, which is sufficiently low to capture the actual dark current of the MIS micro-LEDs. The leakage current densities for M50, M20, M15, and M8 are all ≈3×10^{-8} A cm^{-2}, corresponding to dark currents of ≈550, 90, 50, and 15 fA, respectively. The extremely low leakage current density observed in MIS micro-LEDs with various mesa diameters indicates that the impact of surface defects

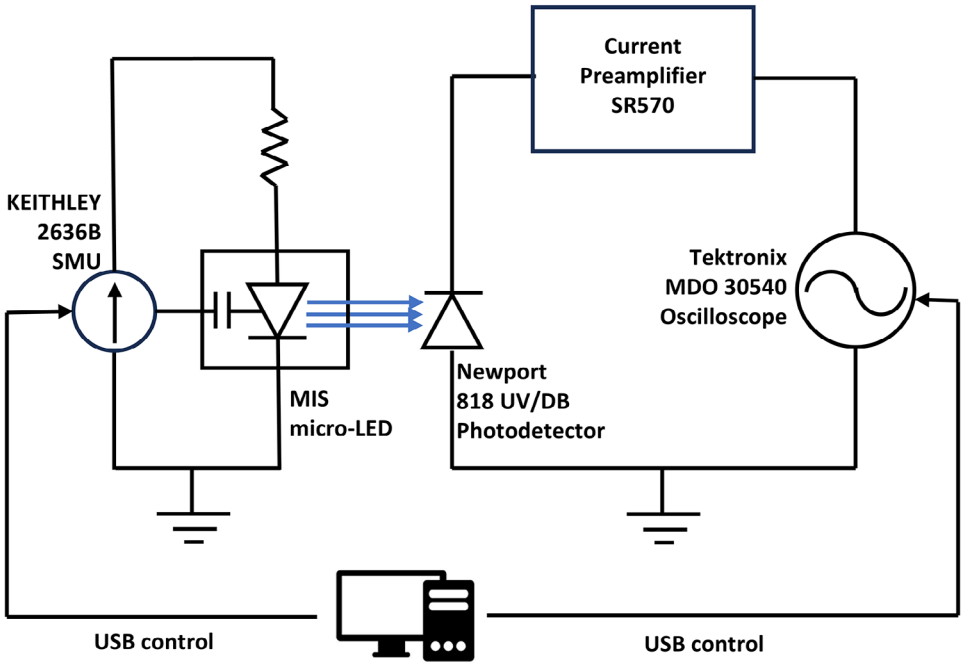

Figure 3. The schematic diagram of the characterization setup for MIS micro-LEDs measurements.

on the sidewalls has been effectively minimized through multiple optimization methods. These include the use of a double-layer hard mask for RIE, an optimized GaN RIE recipe, KOH treatment, and Al_2O_3 sidewall passivation, as detailed in Section 2. Another supporting result is the extremely low ideal factor η_{ideal}, further demonstrating the minimal influence of surface defects on the sidewalls of MIS micro-LEDs. η_{ideal} is a parameter used to describe the deviation of a diode from ideal behavior and is defined as.

$$\eta_{ideal} = \frac{q}{kT}\left(\frac{d}{dV}lnI\right)^{-1} \tag{1}$$

where q is the elementary charge, k is the Boltzmann constant, and T is the room-temperature. In actual measurements, the measured η_{ideal} may be excessively high due to the influence of the diode's parallel resistance at low forward voltages or its series resistance at high forward voltages.[23] Thus, η_{ideal} should be interpreted as the minimum value measured as a function of voltage and current density. The lowest measured η_{ideal} is ≈1.5 at ≈2.55 V (the turn on voltage $V_{turn\text{-}on}$), as shown in Figure 4b. For InGaN/GaN micro-LEDs, η_{ideal} is normally higher than 2.[23] This exceptionally low η_{ideal} demonstrates that extremely low surface recombination has been achieved.

Figure 4c illustrates the effect of sidewall biases on the J–V characteristic curves, using M8 as an example. The J–V curves indicate that sidewall biases do not influence the leakage current from −4 V to a small forward voltage. For M8 with negative sidewall biases, the J–V curves remain close to the J–V curve with zero sidewall bias. However, positive sidewall biases increase the leakage current at forward voltages ($V < V_{turn\text{-}on}$). This increased leakage current is attributed to surface defects-assisted tunneling current, as shown in **Figure 5**.[24] According to our previously published paper,[24] forward voltages on the anodes of devices lower the energy barrier ΔE_0 between the surface defect states and the electron energy states in the active region due to quantum-confined stark effect (QCSE).

In addition, the sidewall biases can adjust the energy level of surface defects, thereby tuning the energy barrier ΔE_0. In the MIS structure, the accumulated charges at the insulator/semiconductor (Al_2O_3/GaN) interface Q_s can be calculated by[25]

$$Q_s = -C_{MIS}\ V_{sidewall} \tag{2}$$

where C_{MIS} is the effective capacitance of MIS structure. On the other hand, Q_s can be calculated using[25]

$$Q_s = \mp\frac{\sqrt{2}\varepsilon_s kT}{qL_D} \times \sqrt{\left[\exp\left(\frac{q\psi_s}{kT}\right) - \frac{q\psi_s}{kT} - 1\right] + \frac{n_i^2}{N_D^2}\left[exp\left(-\frac{q\psi_s}{kT}\right) + \frac{q\psi_s}{kT} - 1\right]} \tag{3}$$

where N_D is the donor concentration in the n-doped active region, n_i is the intrinsic carrier concentration, ε_s is the material permittivity constant, and the Debye length L_D is given by

$$L_D = \sqrt{\frac{kT\varepsilon_s}{N_D q^2}} \tag{4}$$

ψ_s is the surface potential (band bending of the semiconductor), which is the variation of energy level of surface defects as well. Considering that the surface potential ψ_s of the n-doped active

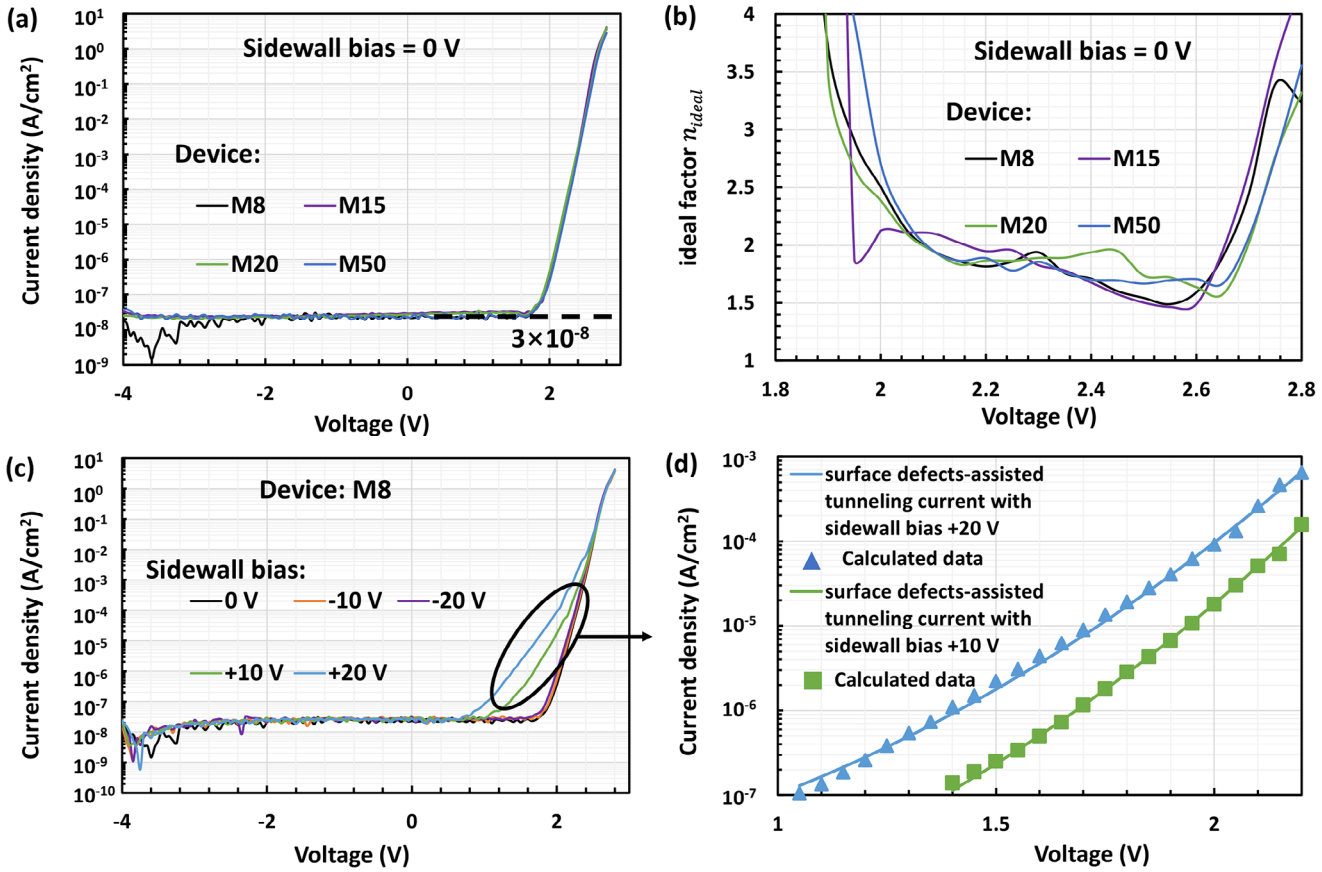

Figure 4. a) The current densities as functions of driving voltages of MIS micro-LEDs with different mesa dimensions at zero sidewall biases; b) The ideal factor η_{ideal} for MIS micro-LEDs with different mesa dimensions; c) The current densities as functions of driving voltages of M8 with different sidewall biases; d) The calculated surface defects-assisted tunneling current densities (the markers) match the measured data of M8 in sub-threshold region (the curves).

region is sufficiently small, Q_s from Equation (3) can be approximated as

$$Q_s \approx -\frac{\varepsilon_s kT}{qL_D}\sqrt{\left(1+\frac{n_i^2}{N_D^2}\right)\left(\frac{q\psi_s}{kT}\right)^2} = -\frac{\varepsilon_s \psi_s}{L_D}\sqrt{1+\frac{n_i^2}{N_D^2}} \quad (5)$$

Substituting Equation (2) into Equation (5) gives

$$\psi_s = \frac{C_{MIS}L_D N_D}{\sqrt{\left(N_D^2+n_i^2\right)\varepsilon_s}} V_{sidewall} \quad (6)$$

Equation (6) describes that the variation of energy level of surface defects ψ_s in the n-doped active region is linearly proportional to the sidewall bias $V_{sidewall}$, provided ψ_s is sufficiently small.

To verify the surface defects-assisted tunneling current shown in Figure 5, the tunneling probability P is given by[24–27]

$$P \sim \exp\left[-\frac{8}{3\hbar}\left(\frac{2\varepsilon_s m^*}{N_T}\right)^{0.5}\Delta E\right] \quad (7)$$

where $\hbar$ is the reduced Planck constant, m^* is the effective mass of electrons, and N_T is the defect-state density. ΔE represents the tunneling barrier between electron energy level and surface defect state level, which can be expressed as[24,28,29]

$$\Delta E = \Delta E_0 - \psi_s - 24\left(\frac{2}{3\pi}\right)^6 \frac{q^2 V^2 m^* L_{QW}^4}{\hbar^2 L_{AR}^2} \quad (8)$$

where L_{QW} is the length of the QWs and L_{AR} is the length of the active region. The last item in Equation (8) is the QCSE item. According to Equations (7) and (8) increasing the forward voltage V reduces ΔE, thereby increasing the surface defects-assisted tunneling current. By using Equations (7) and (8), the calculated surface defects-assisted tunneling current densities outstandingly match the measured J–V data of M8, as shown in Figure 4d. The increasing surface defects-assisted tunneling current of M8 results in an unwanted leakage current in the sub-threshold region. Fortunately, this tunneling current remains much smaller than the total current when M8 is operating above its turn-on voltage. When the driving voltage exceeds 2.55 V ($V_{turn\text{-}on}$), the J–V curves of M8 with positive sidewall biases in Figure 4c show no

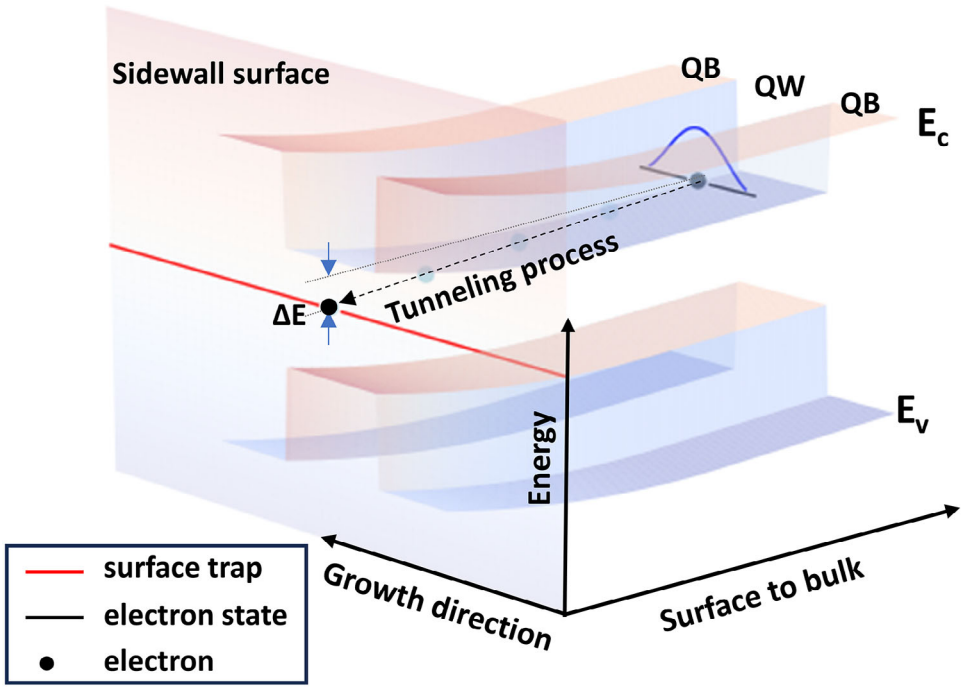

Figure 5. The 3D schematic diagram of the band structure illustrates the surface defects-assisted tunneling recombination process.[24]

significant differences compared to the *J–V* curve with zero sidewall bias.

Moreover, the surface recombination velocity S_0 in n-doped active region is given by[30]

$$S_0 = \frac{S_p}{1 + exp\left[\frac{q(E_t - E_i)}{kT}\right]} \approx S_p exp\left[-\frac{q\left(E_t - E_i\right)}{kT}\right] \tag{9}$$

where S_p is the surface recombination velocity of holes, E_t is the energy level of surface defects, and E_i is the intrinsic fermi level. By incorporating sidewall bending ψ_s from Equation (6) into Equation (9), the new surface recombination velocity S_1 is expressed as

$$S_1 \approx S_p exp\left[-\frac{q\left(E_t - E_i + \psi_s\right)}{kT}\right] = S_0 \exp\left(-\frac{q\psi_s}{kT}\right)$$
$$\approx S_0\left(1 - \frac{q\psi_s}{kT}\right) \tag{10}$$

and

$$\Delta S = S_0 - S_1 = \frac{qC_{MIS}L_D N_D}{\sqrt{\left(N_D^2 + n_i^2\right)\epsilon_s kT}} S_0 V_{sidewall} = KS_0 V_{sidewall} \tag{11}$$

Equation (11) demonstrates that the variation in surface recombination velocity is proportional to the sidewall biases $V_{sidewall}$. For calculation simplicity, we use K as a constant coefficient in the discussion below.

Even though the above discussion provides expressions for ψ_s and ΔS in terms of sidewall biases $V_{sidewall}$, these two parameters are very difficult to experimentally characterize. The most easily quantifiable parameter for MIS micro-LEDs is still the EQE or IQE. To include the effect of surface recombination, the revised ABC model is presented as[31]

$$\eta_{IQE} = \frac{Bn^2}{R} = \frac{Bn^2}{\left(A_0 + \frac{4S}{D}\right)n + Bn^2 + Cn^3} \tag{12}$$

where R, A_0, B, C, S and n are the total recombination rate in micro-LEDs, the bulk SRH recombination coefficient, radiative recombination coefficient, the Auger recombination coefficient, surface recombination and the carrier density, respectively. The total recombination rate R can be calculated by

$$R = \frac{J}{qL_{QW}} = \left(A_0 + \frac{4S}{D}\right)n + Bn^2 + Cn^3 \tag{13}$$

where D is the mesa dimension of the micro-LED. When the mesa dimension D decreases, the ratio r of surface recombination on the sidewall to the active region volume is given by

$$r = S\frac{\pi DL_{QW}n}{\pi\left(\frac{D}{2}\right)^2 L_{QW}} = \frac{4}{D}Sn \tag{14}$$

Therefore, the item $\frac{4S}{D}n$ in the ABC model represents the surface defects-assisted SRH recombination in a micro-LED with mesa dimension D in Equation (12). At low current density,

where Auger recombination can be neglected, the efficiency variation calculated from Equation (12) is given by

$$\Delta IQE = \eta'_{IQE} - \eta_{IQE} = \frac{4\left(S_0 n_0 - S_1 n_1\right)}{DR} \tag{15}$$

where n_0 and n_1 are the carrier densities before and after applying sidewall bias $V_{sidewall}$. Substituting Equation (11) into Equation (15) gives

$$\Delta IQE = \frac{4S_0}{DR}\left(n_0 - n_1 + KV_{sidewall} n_1\right) \tag{16}$$

The carrier density n_0 and n_1 can be derived from Equation (13) as

$$n_{0,1} = \frac{\sqrt{\left(A_0 + \frac{4S_{0,1}}{D}\right)^2 + 4BR} - A_0 - \frac{4S_{0,1}}{D}}{2B} \tag{17}$$

Using the low current density approximation $(A_0 + \frac{4S_{0,1}}{D})^2 \gg 4BR$, substituting Equations (10), (11) and (17) into Equation (16) gives

$$\begin{aligned}\Delta IQE &\approx \frac{\frac{4S_0}{D}}{A_0 + \frac{4S_0}{D}} - \frac{\frac{4\left(1-KV_{sidewall}\right)S_0}{D}}{A_0 + \frac{4(1-K)S_0}{D}} \\ &= \frac{\frac{4KV_{sidewall}S_0}{D}A_0}{\left(A_0 + \frac{4S_0}{D}\right)\left[A_0 + \frac{4\left(1-KV_{sidewall}\right)S_0}{D}\right]}\end{aligned} \tag{18}$$

Equation (18) demonstrates that ΔIQE is constant with a fixed $V_{sidewall}$ and independent of current density at low current density. If $KV_{sidewall} \ll 1$, Equation (18) can be further simplified as

$$\Delta IQE = \frac{4KS_0A_0}{D\left(A_0 + \frac{4S_0}{D}\right)^2} V_{sidewall} \tag{19}$$

In this scenario, ΔIQE is in proportional to the sidewall bias $V_{sidewall}$.

The above calculations quantitatively analyze how the sidewall biases enhance the device efficiency. From the perspective of the underlying physical mechanisms, applying a positive sidewall gate voltage attracts electrons toward the sidewall, resulting in a downward bending of the conduction band edge and electron accumulation at the mesa edge through surface-defect-assisted tunneling recombination. As a result, the surface defect states become filled with electrons. The lifetime of tunneling-assisted recombination is expected to be relatively long, leading to the saturation of surface recombination and a reduction in the availability of defect states for SRH recombination. Consequently, the significant suppression of surface SRH recombination contributes to the improvement of the efficiency.

To verify the above analysis, the EQE performance of M8 with different sidewall biases is exhibited in **Figure 6a**. In Figure 6a, the markers represent the measured results, while the curves depict the simulated results based on our revised ABC model

$$\eta_{EQE} = \eta_{LEE}\frac{Bn}{A_0 + \frac{4\left(S_0 - \frac{\Delta S}{V}V_{sidewall}\right)}{D} + Bn + Cn^2} \tag{20}$$

The fitting parameters are provided in **Table 1**. The light extraction efficiency η_{LEE} was extracted from the ray tracing model in APSYS. From 50 to 8 μm MIS micro-LEDs (D varies from 50 to 8), η_{LEE} varies only slightly (from 70% to 72%). The simulated results from Equation (20) closely match the measured results. The EQE versus J curves indicate that the EQE improvement for M8 is more significant at low current densities.

Figure 6b,c show the EQE variation of M8 at different current densities as sidewall biases increase or decrease. In Figure 6b,c, the increase or decrease in EQE is proportional to the sidewall biases, as described by Equation (19). It can be observed that the EQE enhancement for M8 with positive sidewall biases (2.8 percentage points per +5 V) is more significant than the efficiency degradation with negative sidewall biases (2.3 percentage points per −5 V). This discrepancy arises because, as the active region band bends upward under negative sidewall bias, the effective donor concentration N_D in the active region decreases slightly. As N_D decreases, $\psi_s/V_{sidewall}$ also decreases (according to Equation 6), leading to a reduced $\Delta EQE/V_{sidewall}$. Figure 6b,c further show that as the absolute values of sidewall biases increase, the EQE improvement begins to deviate from a linear relationship slightly. This deviation occurs because the sidewall band bending ψ_s of the active region is no longer sufficiently small, as assumed in Equations (6), (10), and (11). Figure 6b,c also verify that at low current densities, the increased or decreased EQE values remain roughly constant for a fixed sidewall bias, as demonstrated by Equation (18). With a +20 V sidewall bias, the increased EQE values can reach ≈10.7 percentage points at current densities below 3 A cm^{-2}, representing an over 50% increase in the EQE of M8 (from 20.4% to 31.0%) at 0.625 A cm^{-2}. The EQE value of 31.0% at 0.625 A cm^{-2} for M8 is comparable to that of state-of-the-art OLEDs (Figure 1b). The EQE improvement demonstrates that the MIS structure can significantly enhance the EQE of micro-LEDs, especially at low operating current densities. The maximum EQE value of M8 is ≈53.9% at 23.3 A cm^{-2}, which, to the best of our knowledge, exceeds any reported peak EQE values for published micro-LEDs with mesa dimensions below 20 μm.

In addition to EQE, Figure S2 (Supporting Information) presents the wall-plug efficiency (WPE) of the M8 device as a function of current density, both without sidewall bias and with a +20 V sidewall bias. At low current densities, the WPE values closely follow the EQE trend. With a +20 V sidewall bias, the WPE increases from 21.1% to 32.2% at 0.625 A cm^{-2}, corresponding to an ≈52% improvement. The low gate current of the MIS sidewall electrode (≈2 pA) has a negligible impact on WPE when the MIS micro-LED is operating. Notably, the maximum WPE of the M8 device with +20 V bias reaches ≈50.8% at 7.81 A cm^{-2}, which is also the one of the highest reported WPE value for InGaN/GaN micro-LEDs.

To further validate the reliability of the MIS structure and the revised ABC model (Equation 20), Figure 6d,e show the EQE values as functions of current densities for MIS micro-LEDs with

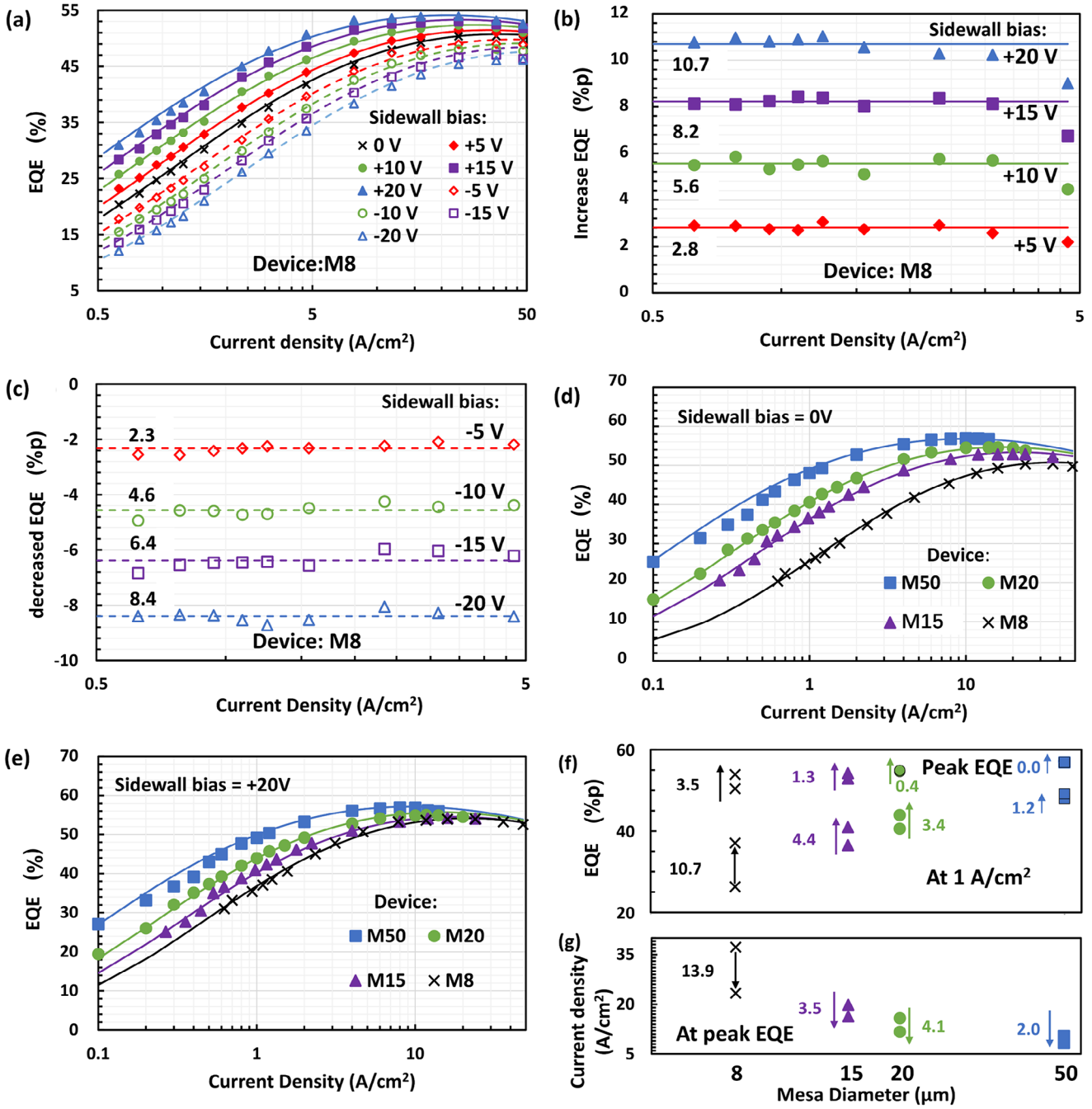

Figure 6. a) The EQE values as functions of current densities of M8 with different sidewall biases. b) The increased EQE of M8 with different positive sidewall biases at different current densities. c) The decreased EQE of M8 with different negative sidewall biases at different current densities. d) The EQE values as functions of current densities of MIS micro-LEDs with different mesa diameters at 0 V sidewall bias and e) at 20 V sidewall bias. f) The increased EQE values of MIS micro-LEDs with different mesa diameters at 1 A cm^{-2} and the peak. g) The decreased current densities of MIS micro-LEDs with different mesa diameters at peak EQE. The markers are the measured results, and the curves are the simulated results based on Equation (20) in Figures (a), (d), and (e).

different mesa diameters at 0 and +20 V sidewall biases. The simulated results from Equation (20) closely align with the measured data. The revised ABC model (Equation 20) and the fitting parameters presented in Table 1 are well suited for describing the characteristics of our micro-LEDs with different sizes. With a +20 V positive bias applied to the sidewall electrodes, the EQE performance of M8 approaches that of M15 and M20. At 1 A cm^{-2}, the increased EQE of M8 (10.7% points) is more than double the increase observed in M15 and M20, as exhibited in Figure 6f. However, at the peak EQE, the rise in EQE of M8 is only 3.5% points, while the increase in EQE of M20 can be considered negligible. Figure 6f reaffirms that the EQE improvement for MIS

Table 1. The fitting parameters in the revised ABC model for various dimensions.

Bulk SRH recombination coefficient	Radiative recombination coefficient	Auger recombination coefficient	Light extraction efficiency	Surface recombination velocity	Increase in surface recombination velocity per sidewall bias
A_0 (s^{-1})	B ($cm^3 s^{-1}$)	C ($cm^6 s^{-1}$)	η_{LEE}	S (m/s)	$\Delta S/V$ ($m\ s^{-1} V^{-1}$)
3.2×10^6	1.3×10^{-10}	4×10^{-29}	70–72%	31	0.78

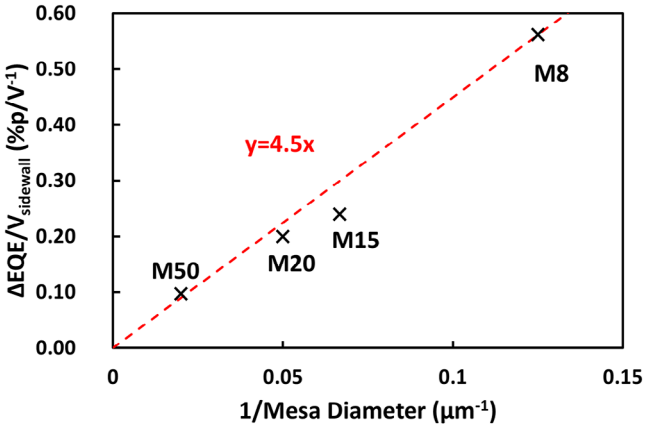

Figure 7. The $\Delta EQE/V_{sidewall}$ of MIS micro-LEDs as a function of the reciprocal of the mesa diameter.

micro-LEDs is more pronounced at low current densities. This is advantageous, as most miniature high-resolution displays operate at low current densities, as discussed in the introduction. Additionally, applying a +20 V sidewall bias reduces the current densities at peak EQE for MIS micro-LEDs with different mesa diameters, as illustrated in Figure 6g. The largest reduction in current density at peak EQE, 13.9 A cm^{-2}, is observed for M8, significantly more significant than the reductions for M15 and M20. This result highlights that MIS structures are more effective for micro-LEDs with small mesa diameters.

To summarize and predict the efficiency improvement of MIS micro-LEDs with different sizes, an empirical formula is proposed. **Figure** 7 shows the increase in EQE per unit sidewall bias as

$$\frac{\Delta EQE}{V_{sidewall}} = \frac{4.5\%p}{MesaDiameter} \tag{21}$$

which predicts that MIS structures can provide even greater EQE improvements for smaller MIS micro-LEDs.

4. Conclusion

This work addresses the significant EQE degradation issue in InGaN/GaN micro-LEDs as device sizes are reduced to the micrometer scale, which is a critical bottleneck for their widespread application. By introducing an MIS structure on the sidewall of the device mesa, we demonstrated an effective method to suppress surface nonradiative recombination and enhance EQE. Using advanced fabrication techniques, MIS InGaN/GaN micro-LEDs with various mesa diameters were fabricated, and the device performance was characterized. The measured J–V curves revealed that applying a positive sidewall bias to the sidewall electrode of the MIS structure effectively reduces the energy difference between surface defect states and electron energy states in the active region. This reduction decreases the surface recombination velocity of the MIS micro-LEDs. Detailed quantitative analyses explained the underlying mechanisms and calculated the relationship between the applied sidewall biases and the variation of EQE values in MIS micro-LEDs. The increase or decrease in the measured EQE was found to be approximately proportional to the magnitude of the positive or negative sidewall bias applied to the MIS micro-LEDs in the range of −20 to +20 V. An analytical model based on the ABC model was developed to explain the experimental results, which closely match the measured data. For MIS micro-LEDs with an 8 μm mesa dimension, the EQE improved from 20% to 30.7% (an increase of 10.7% points) at 0.625 A cm^{-2} by applying a +20 V sidewall bias. This EQE value is comparable to those of state-of-the-art OLEDs, showing the great potential of MIS micro-LEDs for miniature high-resolution display applications. Furthermore, the maximum EQE of the 8 μm MIS micro-LED was measured to be ≈53.9% at an injection current density of 23.3 A cm^{-2}, which is the reported highest EQE among state-of-the-art InGaN/GaN micro-LEDs to date.

Supporting Information

Supporting Information is available from the Wiley Online Library or from the author.

Acknowledgements

This research was supported by the Natural Sciences and Engineering Research Council of Canada (NSERC), the Ontario Centres for Excellence (OCE), the Canada Foundation of Innovation (CFI), and the University of Waterloo. The authors would also like to thank Dr. Farshid Karbassian of Vuereal for his valuable suggestions.

Conflict of Interest

The authors declare no conflict of interest.

Data Availability Statement

The data that support the findings of this study are available within this article in the form of figures. The related data tables are available from the corresponding author upon reasonable request.

Keywords

GaN micro-LEDs, high EQE, low surface recombination velocity, metal-insulator-semiconductor devices

Received: April 7, 2025
Revised: July 23, 2025
Published online: August 4, 2025

[1] J. Wang, L. Wang, W. Zhao, Z. Hao, Y. Luo, *Appl. Phys. Lett.* **2010**, *97*, 201112.
[2] J. Cho, E. Fred Schubert, J. K. Kim, *Laser Photonics Rev.* **2013**, *7*, 408.
[3] M.-H. Kim, M. F. Schubert, Q. Dai, J. K. Kim, E. F. Schubert, J. Piprek, Y. Park, *Appl. Phys. Lett.* **2007**, *91*, 183507.
[4] C.-H. Dong, L. He, Y.-F. Xiao, V. R. Gaddam, S. K. Ozdemir, Z.-F. Han, G.-C. Guo, L. Yang, *Appl. Phys. Lett.* **2009**, *94*, 231119.
[5] Y. Zhang, Yun, Y. A. Yin, *Appl. Phys. Lett.* **2011**, *99*, 221103.
[6] Y. Zou, J. Hu, M. Yu, J. Miao, Z. Xie, Y. Qiu, X. Cao, C. Yang, *Adv. Mater.* **2022**, *34*, 2201442.
[7] W. Yang, J. Miao, F. Hu, Y. Zou, C. Zhong, S. Gong, C. Yang, *Adv. Funct. Mater.* **2023**, *33*, 2213056
[8] N. Li, Z. Chen, C. Zhou, F. Ni, Z. Huang, X. Cao, C. Yang, *Adv. Mater.* **2023**, *35*, 2300510
[9] G.-Z. Lu, Q. Zhu, L. Liu, Z.-G. Wu, Y.-X. Zheng, L. Zhou, J.-L. Zuo, H. Zhang, *ACS Appl. Mater. Interfaces* **2019**, *11*, 20192.
[10] Y. H. Lee, W. Lee, T. Lee, J. Jung, S. Yoo, M. H. Lee, *Chem. Eng. J.* **2023**, *452*, 139387.
[11] K. Kumada, H. Sasabe, M. Matsuya, N. Yoshida, K. Hoshi, T. Nakamura, H. Nemma, J. Kido, *J. Mater. Chem. C* **2023**, *11*, 13782.
[12] J. Zhang, M. Wu, D. Zheng, J. Zhao, J. Yu, *Appl. Phys. Lett.* **2024**, *125*, 121102.
[13] C. Ou, Y.-C. Qiu, C. Cao, H. Zhang, J. Qin, Z.-L. Tu, J. Shi, Z.-G. Wu, *Inorg. Chem. Front.* **2023**, *10*, 1018.
[14] A. Pandey, J. Min, M. Reddeppa, Y. Malhotra, Y. Xiao, Y. Wu, K. Sun, Z. Mi, *Nano Lett.* **2023**, *23*, 1680.
[15] L. Wang, X. Zhang, F. Chen, *Laser Photonics Rev.* **2021**, *15*, 2000406.
[16] Y. Liu, M. Zhanghu, F. Feng, Z. Li, K. e. Zhang, H. S. Kwok, Z. Liu, *Opt. Express* **2023**, *31*, 17557.
[17] M. S. Wong, C. Lee, D. J. Myers, D. Hwang, J. A. Kearns, T. Li, J. S. Speck, S. Nakamura, S. P. DenBaars, *Appl. Phys. Express* **2019**, *12*, 097004.
[18] M. S. Wong, D. Hwang, A. I. Alhassan, C. Lee, R. Ley, S. Nakamura, S. P. DenBaars, *Opt. Express* **2018**, *26*, 21324.
[19] D. Hwang, A. Mughal, C. D. Pynn, S. Nakamura, S. P. DenBaars, *Appl. Phys. Express* **2017**, *10*, 032101.
[20] A. Tanide, S. Nakamura, A. Horikoshi, S. Takatsuji, M. Kohno, K. Kinose, S. Nadahara, K. Ishikawa, M. Sekine, M. Hori, *J. Vac. Sci. Technol. B* **2019**, *37*, 021209.
[21] D. Hwang, Ph.D., University of California, Santa Barbara, California, USA **2018**.
[22] Y. Yang, X. A. Cao, *Meas. Phenom.* **2009**, *27*, 2337.
[23] E. F. Schubert, *Light-Emitting Diodes*, Rensselaer Polytechnic Institute, Troy, New York, USA **2018**.
[24] J. Yin, E. Fathi, H. Z. Siboni, C. Xu, D. Ban, *Appl. Phys. Lett.* **2021**, *118*, 021105.
[25] S. M. Sze, K. K. NG, *Physics of Semiconductor Devices*, 3rd ed., Wiley, Hoboken, NJ, USA **2006**.
[26] S. Huang, Y. Xian, B. Fan, Z. Zheng, Z. Chen, W. Jia, H. Jiang, G. Wang, *J. Appl. Phys.* **2011**, *110*, 064511.
[27] E. Liu, B. Zhu, J. Luo, *Semiconductor Physics*, 4th ed. National Defense Industry Press, Peking, China **2006**.
[28] D. A. B. Miller, D. S. Chemla, T. C. Damen, A. C. Gossard, W. Wiegmann, T. H. Wood, C. A. Burrus, *Phys. Rev. Lett.* **1984**, *53*, 2173.
[29] D. A. B. Miller, D. S. Chemla, T. C. Damen, A. C. Gossard, W. Wiegmann, T. H. Wood, C. A. Burrus, *Phys. Rev. B* **1985**, *32*, 1043
[30] W. T. R. W. Shockley, W. T. Read Jr, *Phys. Rev.* **1952**, *87*, 835
[31] J. M. Smith, R. Ley, M. S. Wong, Y. H. Baek, J. H. Kang, C. H. Kim, M. J. Gordon, S. Nakamura, J. S. Speck, S. P. DenBaars, *Appl. Phys. Lett.* **2020**, *116*, 071102.